Geometry dependence of stellarator turbulence

H. E. Mynick,[1] P. Xanthopoulos,[2] and A. H. Boozer[3]
[1]*Plasma Physics Laboratory, Princeton University, Princeton, New Jersey 08543, USA*
[2]*Max-Planck-Institut für Plasmaphysik, Teilinstitut Greifswald, 17491 Greifswald, Germany*
[3]*Department of Applied Physics and Mathematics, Columbia University, New York, New York 10027, USA*

(Received 13 July 2009; accepted 14 October 2009; published online 10 November 2009)

Using the nonlinear gyrokinetic code package GENE/GIST [F. Jenko, W. Dorland, M. Kotschenreuther, and B. N. Rogers, Phys. Plasmas **7**, 1904 (2000); P. Xanthopoulos, W. A. Cooper, F. Jenko, Yu. Turkin, A. Runov, and J. Geiger, *ibid.* **16**, 082303 (2009)], we study the turbulent transport in a broad family of stellarator designs, to understand the geometry dependence of the microturbulence. By using a set of flux tubes on a given flux surface, we construct a picture of the two-dimensional structure of the microturbulence over that surface and relate this to relevant geometric quantities, such as the curvature, local shear, and effective potential in the Schrödinger-like equation governing linear drift modes. © *2009 American Institute of Physics*. [doi:10.1063/1.3258848]

The concept of "transport-optimized stellarators" (for an overview see, e.g., Ref. 1) aims at mitigating the neoclassical (nc) losses to the point where anomalous transport becomes dominant over most of the plasma column. Attention is now turning to understanding the effects of three-dimensional (3D) geometry on microturbulence,[2–6] aided by nonlinear gyrokinetic (gk) codes valid for 3D. Supported by the scant, albeit promising, existing findings in this area, we attempt to identify key geometrical factors which contribute to the development and, subsequently, control of turbulent transport levels. In this letter, we employ the GENE/GIST code package[7,8] and apply its unique capability of determining turbulence properties for a 3D VMEC equilibrium[9] to a wide representative family of optimized stellarator designs (plus one reference axisymmetric system), to understand the geometry dependence of ion-temperature-gradient (ITG) turbulence.

Existing 3D nonlinear gk codes are "flux tube" codes,[10] yielding a picture of the turbulence along a particular field line, a one-dimensional (1D) structure. To better relate such results to the full geometry, we follow a novel procedure, to construct the two-dimensional (2D) structure of the turbulence over a flux-surface by combining results for a set of such field lines on that flux surface and relate this structure to relevant geometric quantities, including the curvature, local shear, and effective potential $V_{\mathrm{eff}}(z)$ in the Schrödinger-like equation governing linear drift modes.

The volume of a torus is conveniently parametrized by flux coordinates $\mathbf{x}=(\psi,\theta,\zeta)$, with $2\pi\psi$ the toroidal flux within a flux surface, and θ and ζ the poloidal and toroidal azimuths, chosen so that the magnetic field may be written $\mathbf{B}=\nabla\alpha\times\nabla\psi_p$, with $2\pi\psi_p(\psi)$ the poloidal flux, $\alpha\equiv\zeta-q\theta$, and $q(\psi)\equiv\iota^{-1}$ the tokamak safety factor. In its local mode of operation, GENE simulates plasma turbulence in a field-line following coordinate system (x,y,z) within a flux tube surrounding a specified field line, with $z=\theta$ the coordinate along a field line, $x\equiv r-r_0$, with $r(\psi)\equiv(2\psi/B_a)^{1/2}$ a minor radial variable with units of length, r_0 the value of r on the chosen flux surface, B_a a normalizing magnetic field strength, and $y\equiv-r_0\iota_0\alpha$ the in-surface Clebsch coordinate with units of length, satisfying $\mathbf{B}=B_a\nabla x\times\nabla y$. z typically runs for 1 full poloidal transit, and (quasi-)periodic boundary conditions are imposed in all three directions. The simulations discussed here all compute collisionless electrostatic turbulence, assuming adiabatic electrons, with parameters $a/L_n\equiv-a\partial_r n/n=0$, $a/L_{Ti}\equiv-a\partial_r T_i/T_i=3$, $r_0/a\simeq0.7$, $\tau\equiv T_e/T_i=1$, $\rho_s/L_y=0.05/2\pi$, and $L_x=L_y$, with $L_{x,y}$ the box size in the x and y directions, a the value of r at the edge, $\rho_s\equiv c_s/\Omega_i$, $c_s\equiv(T_e/M_i)^{1/2}$ the sound speed, and Ω_i the ion gyrofrequency. $N_x\times N_y\times N_z=64\times96\times(96\text{ or }128)$ grid points were employed in the x, y, and z directions, and $N_{v_\parallel}\times N_\mu=32\times8$ points in velocity space.

The configurations studied include a representative from each of the three principal approaches to nc transport optimization,[1] National Compact Stellarator Experiment (NCSX),[11] a three field-period ($N=3$) quasiaxisymmetric (QA) design, Helically Symmetric Experiment (HSX),[12] an $N=4$ quasihelically symmetric design, and W7X (Wendelstein VII-X),[13] an $N=5$ quasi-isodynamic/quasi-omnigenous (QI/QO) design. We also simulate NCSX_sym, a fully axisymmetric (2D) equilibrium obtained from the NCSX geometry by dropping all the nonaxisymmetric Fourier components. We construct a 2D picture of the time-averaged rms turbulent potential amplitude $\langle\phi\rangle(\theta,\zeta|r_0)$ over the flux surface at $r=r_0$ from a set of M flux-tube GENE simulations. The simulations for tubes $j=0,1,\ldots,M-1$ are evenly spaced over a half field period, $N\alpha_0=0,\pi/(M-1),\ldots,\pi$. Each simulation produces the turbulent amplitude $\langle\phi\rangle(z|r_0,N\alpha_0)$. The value of $\langle\phi\rangle$ in the other half field period [tubes labeled $j=-1,\ldots,-(M-1)$] is obtained from the tubes in the simulated half period via stellarator symmetry, $\langle\phi\rangle(-\theta,-\zeta|r_0)=\langle\phi\rangle(\theta,\zeta|r_0)$, or $\langle\phi\rangle(-z|r_0,-N\alpha_0)=\langle\phi\rangle(z|r_0,N\alpha_0)$. The 2D strip for a single field period is then replicated N times to cover a complete flux surface. The construction for any other relevant physical quantity is essentially the same.

Figure 1(a) shows a 1D plot of $\langle\phi\rangle(z|r_0,N\alpha_0)$ for $M=3$ flux tubes for NCSX, for $N\alpha_0=0$ (blue), $\pi/2$ (green), and

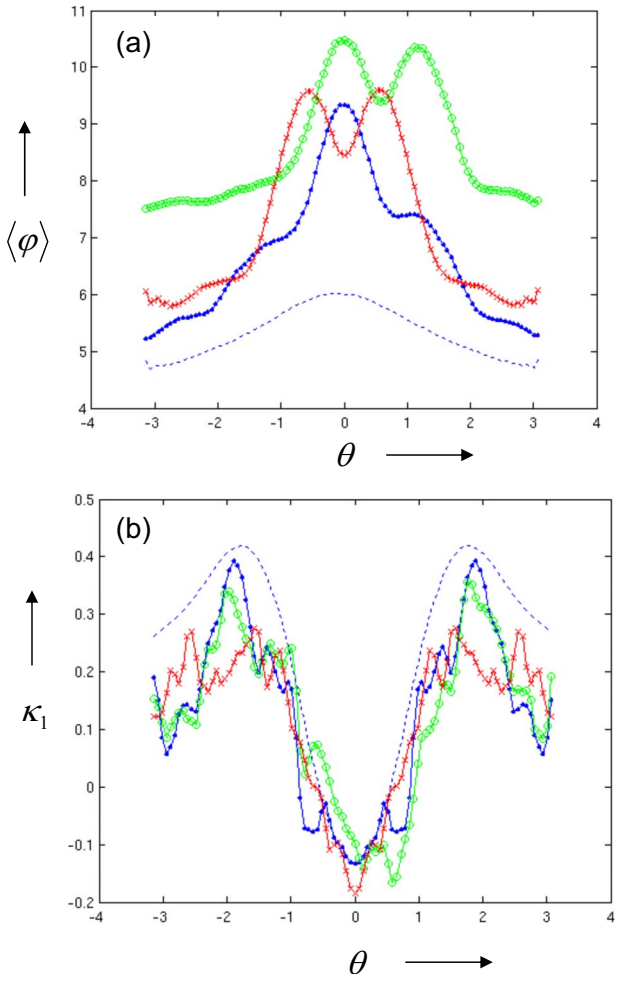

FIG. 1. (Color online) (a) Averaged turbulent potential $\langle\phi\rangle(z=\theta)$ and (b) curvature $\mathcal{K}_1(z=\theta)$ for NCSX_sym (dashed line) and NCSX (solid line). NCSX tubes $j=0$, 1, and 2 are colored blue (points), green (circles), and red (crosses), respectively.

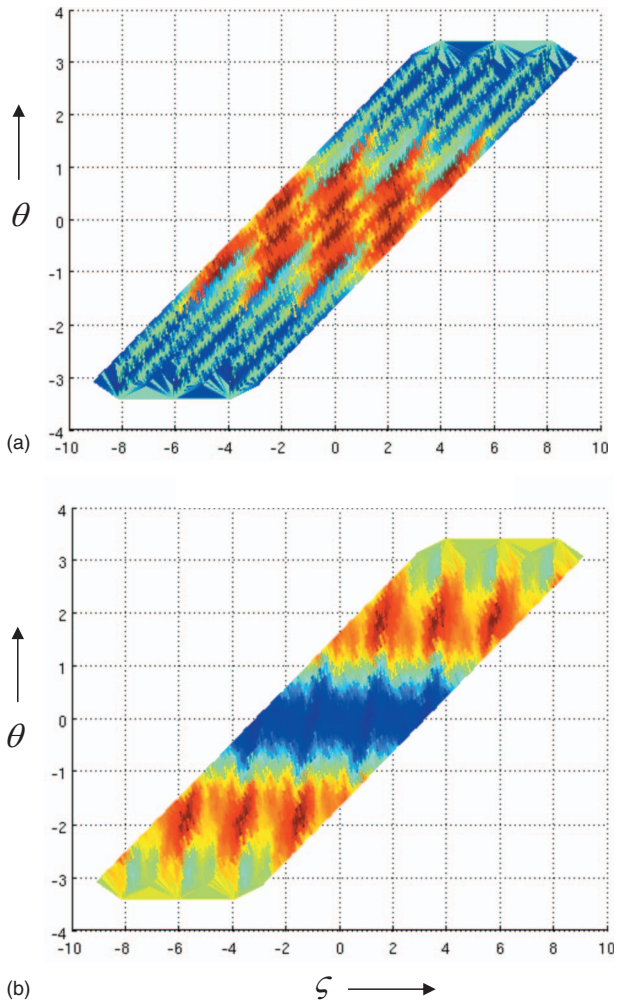

FIG. 2. (Color) (a) $\langle\phi\rangle(\theta,\zeta)$ and (b) $\mathcal{K}_1(\theta,\zeta)$ for NCSX.

π (red), along with a single flux tube (dashed blue) for NCSX_sym (all tubes are equivalent in a 2D torus). Figure 1(b) shows the corresponding plot for the radial curvature component $\mathcal{K}_1(z|r_0,N\alpha_0)=\boldsymbol{\kappa}\cdot\mathbf{e}_x$ whose negative values indicate "bad curvature"[14] ($\mathbf{e}_x$ is the covariant basis vector).

In Fig. 2(a) the 2D plot $\langle\phi\rangle(\theta,\zeta)$ is composed from the NCSX tubes in Fig. 1(a), with red being large values and blue low values. Figure 2(b) shows the corresponding plot for $\mathcal{K}_1$. For NCSX_sym, as expected, one sees in Fig. 1 that $\langle\phi\rangle$ balloons toward the outboard side ($\theta=0$), where $\mathcal{K}_1$ is worst (most negative). As one might also expect, $\langle\phi\rangle$ and $\mathcal{K}_1$ for NCSX_sym look like axisymmetrized versions of those in Figs. 1 and 2.

Shown in Fig. 3 are the 1D plots $\langle\phi\rangle$ and $\mathcal{K}_1$ for W7X, whose toroidal amplitude ϵ_t is comparable to its helical amplitude ϵ_h, characteristic of QO/QI systems. While B and $\mathcal{K}_1$ have a variation on the more rapid helical scale length L_h, the helical wells these produce in the mode equation's effective potential $V_{\rm ef}$ are insufficient to localize an ITG mode, leaving the longer, toroidal well to provide the dominant localization.

A similar statement holds for HSX, whose magnetic field strength $B(\mathbf{x})$ is helically symmetric to better than one part in 400, ($\epsilon_t \ll \epsilon_h$). Here, while one might expect the toroidal ballooning evident in NCSX and NCSX_sym to be replaced by an analogous ballooning within a helical ripple period, as for W7X, L_h is too narrow to localize $\langle\phi\rangle$, as seen in Fig. 4, and as a result the turbulence in each tube still balloons toward $\theta=0$, though not as much as for a tokamak or QA system. This surprising finding is experimentally supported by HSX probe measurements.[15]

For each of these configurations, the region of maximum $\langle\phi\rangle$ and local heat flux Q_i occurs where $\mathcal{K}_1$ is most negative, which is around $(\theta,N\alpha_0)\simeq(0,0)$, i.e., on the outboard side around the device "corners." The variation along a field line of the heat flux $Q_i(\theta|N\alpha_0)$ from GENE strongly resembles the variation of $\langle\phi\rangle$, qualitatively given by the scaling $Q_i \sim \Sigma_{\mathbf{k}} k_y^2|\phi|^2$, suggesting weak turbulence. The factor of k_y^2 here removes the contribution to Q_i from low-k_y fluctuations, which examination of the GENE output spectrum $\phi(k_x,k_y,z)$ shows is dominated by zonal flows ($k_y=0$), which give the appreciable minimum value ϕ_0 observed in Figs. 1–4. The tube-averaged flux $\bar{Q}_i(N\alpha_0)=-n_0\bar{\chi}_i\langle\nabla T_{i0}\cdot\nabla x\rangle$ or anomalous diffusivity $\bar{\chi}_i$ varies little with tube in NCSX, behaving in this sense like a truly 2D system (though the metric profiles in different tubes differ considerably for QAs), while they vary a good deal ($\bar{\chi}_{\rm max}/\bar{\chi}_{\rm min}\simeq 3.2$) for W7X, where different

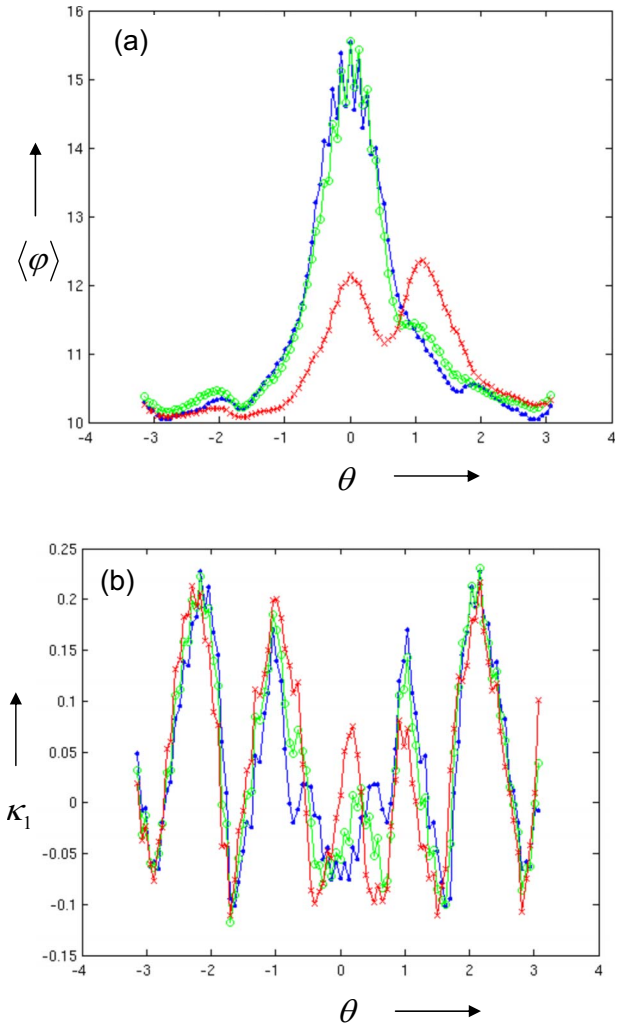

FIG. 3. (Color online) (a) $\langle\phi\rangle(z=\theta)$ and (b) $\mathcal{K}_1(z=\theta)$ for W7X. Colors and markers as in Fig. 1.

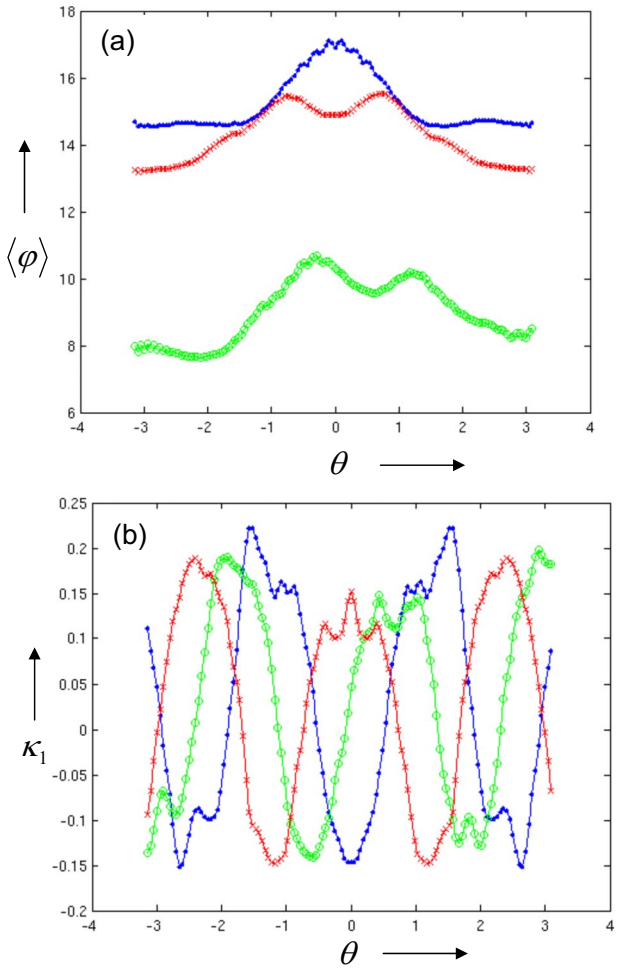

FIG. 4. (Color online) (a) $\langle\phi\rangle(z=\theta)$ and (b) $\mathcal{K}_1(z=\theta)$ for HSX. Colors and markers as in Fig. 1.

tubes have quite different profiles of B and $\mathcal{K}_1$. Flux-surface averaging by summing over the tube results via $\bar{\bar{\chi}}_i = \Sigma_{j=-1}^{2} \bar{\chi}_i(j)/4$, one finds $\bar{\bar{\chi}}_i/\chi_{\mathrm{gB}} \simeq 7.9$, 9.9, 17, and 10.4 for NCSX_sym, NCSX, W7X, and HSX, respectively, where $\chi_{\mathrm{gB}} \equiv \rho_s^2 c_s/a$ is the gyro-Bohm diffusivity. Simulations using other particular plasma parameters, or including the effects of kinetic electrons or the ambipolar electric field, may be expected to change the particular values and ordering of the results for these configurations. What is more noteworthy is that all configurations provide values comparable to a tokamak and to each other.

It has been observed[3] that $\langle\phi\rangle(\theta)$ for ITG turbulence resembles the structure of the linear modes.[16] One may obtain an equation[17] for the linear modes $\phi(\theta)$ from the quasineutrality condition $0 = g_e/\tau + g_i$, with response function g_s equal to $k^2\lambda_s^2$ times the linear susceptibility, yielding

$$0 = g_e/\tau + 1 - \left\langle J_0^2 \frac{\omega - \omega_{*i}^f}{\omega - k_\parallel v_\parallel - \omega_D} \right\rangle_v \simeq C(\omega) + D(\omega)(qRk_\parallel)^2, \quad (1)$$

cubic in mode frequency ω, with velocity-space average $\langle\cdots\rangle$, $\omega_*^f \equiv \omega_*[1+\eta(u^2-3)/2]$, $u \equiv v/v_T$, thermal velocity v_T, diamagnetic and drift frequencies $\omega_* \equiv -ck_\theta \kappa_n T/(eB)$, $\omega_D = \omega_d(u_\perp^2/2 + u_\parallel^2)$, $\omega_d \equiv cT_i/(e_i B^3)\mathbf{B}\times\nabla B\cdot\mathbf{k}_\perp$, $C(\omega) \equiv (c_0 + \omega^{-1}c_1 + \omega^{-2}c_2)$, $D(\omega) \equiv (\omega^{-2}d_2 + \omega^{-3}d_3)$, and coefficients c_{0-2}, d_{2-3} collecting terms in powers of ω and $k_\parallel$, e.g., $c_0 \equiv g_e/\tau + 1 - I_0(b_i)e^{-b_i}$. For adiabatic electrons, $g_e = 1$.

The shape of $V_{\mathrm{ef}} \equiv C(\omega)/D(\omega)$, shown in Fig. 5 for a single tube ($j=2$) for each of the four geometries, is dominated by that of $\mathcal{K}_1$, coming from the drift term ($\propto \omega_D/\omega$) from Eq. (1). Using the replacement $ik_\parallel \to \nabla_\parallel = (B\mathcal{J})^{-1}\partial_\theta$ in Eq. (1), with Jacobian $\mathcal{J} \equiv 1/\nabla\alpha\times\nabla\psi_p\cdot\nabla\theta \equiv 1/B^\theta$, a Schrödinger-like mode equation is obtained for ϕ along a field line, $0 = [V_{\mathrm{ef}} - (qRB^\theta/B)\partial_\theta(qRB^\theta/B)\partial_\theta)]\phi(\theta)$, in which curvature enters through V_{ef}.

The local shear $s_l = \partial_\theta(g^{xy}/g^{xx})$ (with g^{ij} the components of the metric tensor) enters Eq. (1) through locally modifying both $k_\parallel(\theta)$, and $k_\perp^2(\theta)$ through radial wavenumber $k_x(\theta)$. In Fig. 6 s_l in NCSX and NCSX_sym are compared. As for other stellarators, the much stronger shaping for NCSX makes $|s_l|$ substantially larger and more structured than for a 2D system like NCSX_sym. One might expect spikes in s_l to bound modes more than would occur just through the action of V_{ef}, since s_l causes $k_\parallel$ or k_x to locally appreciably deviate from 0, enhancing Landau damping, as well as reducing the mode radial extent, similar to the function performed nonlin-

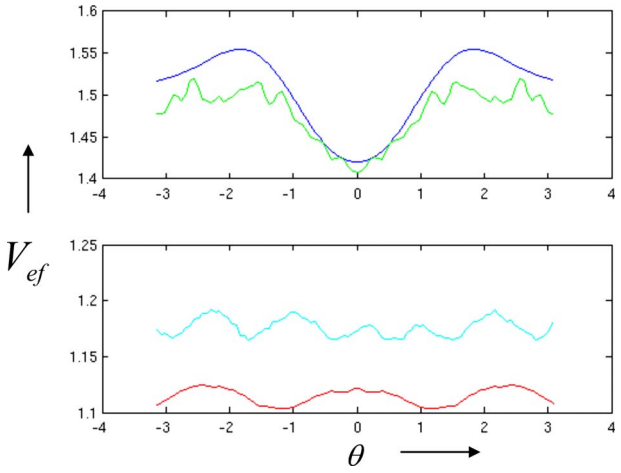

FIG. 5. (Color online) Effective potential $V_{ef}(z=\theta)$ for tube $j=2$ of (from top to bottom) NCSX_sym (blue), NCSX (green), W7X (cyan), and HSX (red), for $k_y\rho_s=0.25$.

early by zonal flows. Evidence for this may be seen in comparing the spikes in s_l in Fig. 6 with the restrictions and dimples in $\langle\phi\rangle$ for NCSX in Fig. 1(a). Further support is found by creating an artificial configuration, NCSX_s, obtained from NCSX by artificially doubling s_l by doubling g^{xy}, adjusting g^{yy} to preserve the field alignment constraint, and consistently modifying $\mathcal{K}_1$, which implicitly contains g^{xy}. $\langle\phi\rangle(\theta)$ in NCSX_s resembles that of NCSX, but substantially more localized, restricted by the increased peaks in $s_l(\theta)$, with $Q_i(\theta)$ correspondingly narrowed and $\bar{Q}_i$ reduced by about 30%.

Summarizing, we have examined the structure of microturbulence in a broad family of transport-optimized toroidal systems using the gk code GENE. Visualizing this, and its relation to important geometric quantities, is facilitated by

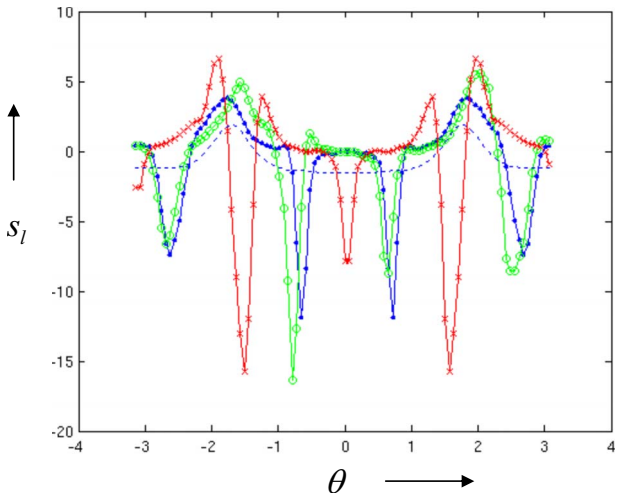

FIG. 6. (Color online) Local shear $s_l(z=\theta)$ for NCSX_sym (dashed line) and NCSX (solid line). Colors and markers as in Fig. 1.

the construction of a 2D picture of these over a flux surface from the 1D information a flux-tube code provides. Two such quantities, $\mathcal{K}_1$ and s_l, are seen to be important for ITG turbulence in determining the similar structures of the heat flux Q_i, and of the varying (nonzonal flow) portion of the turbulent amplitude $\langle\phi\rangle$, from both the simulation results, and because both input quantities are operative in the linear mode equation, whose solutions ϕ are observed to resemble $\langle\phi\rangle$ and Q_i. For each stellarator, $\langle\phi\rangle$ and Q_i are seen to peak toward the outboard side near the device corners (where $\mathcal{K}_1$ is worst), manifesting a toroidal ballooning structure, which is modulated by the helical ripples, but not enough to localize modes within them, even for HSX. Further improvements to the present results are planned, e.g., incorporating the effect of an ambipolar electric field, and including kinetic electrons, which provide the trapped electron drive, changing the mode characteristics.[14] The relatively simple relationship between the GENE outputs $\langle\phi\rangle$ and Q_i, and identifiable inputs like $\mathcal{K}_1$ and s_l, which can be quickly computed, suggests an optimization may be done, minimizing a semianalytic proxy for Q_i, involving those inputs through solving the mode equation, to obtain a geometry which seeks to minimize the turbulent transport.

The authors are grateful to F. Jenko, F. Merz, J. Talmadge, and E. Valeo for valuable discussions. This work has been supported by U.S. Department of Energy Contract No. DE-AC02-09CH11466.

[1] H. E. Mynick, Phys. Plasmas **13**, 058102 (2006).
[2] T.-H. Watanabe, H. Sugama, and S. Ferrando-Margalet, Phys. Rev. Lett. **100**, 195002 (2008).
[3] P. Xanthopoulos, F. Merz, T. Goerler, and F. Jenko, Phys. Rev. Lett. **99**, 035002 (2007).
[4] H. Sugama and T.-H. Watanabe, Phys. Plasmas **16**, 056101 (2009).
[5] W. Guttenfelder, J. Lore, D. T. Anderson, F. S. B. Anderson, J. M. Canik, W. Dorland, K. M. Likin, and J. N. Talmadge, Phys. Rev. Lett. **101**, 215002 (2008).
[6] S. Marsen, M. Otte, and F. Wagner, Contrib. Plasma Phys. **48**, 467 (2008).
[7] F. Jenko, W. Dorland, M. Kotschenreuther, and B. N. Rogers, Phys. Plasmas **7**, 1904 (2000).
[8] P. Xanthopoulos, W. A. Cooper, F. Jenko, Yu. Turkin, A. Runov, and J. Geiger, Phys. Plasmas **16**, 082303 (2009).
[9] S. P. Hirshman, W. I. van Rij, and P. Merkel, Comput. Phys. Commun. **43**, 143 (1986).
[10] M. A. Beer, S. C. Cowley, and G. W. Hammett, Phys. Plasmas **2**, 2687 (1995).
[11] G. H. Neilson, M. C. Zarnstorff, J. F. Lyon, and the NCSX Team, J. Plasma Fusion Res. **78**, 214 (2002).
[12] J. N. Talmadge, V. Sakaguchi, F. S. B. Anderson, D. T. Anderson, and A. F. Almagri, Phys. Plasmas **8**, 5165 (2001).
[13] G. Grieger, W. Lotz, P. Merkel, J. Nührenberg, J. Sapper, E. Strumberger, H. Wobig, R. Burhenn, V. Erckmann, U. Gasparino, L. Giannone, H. J. Hartfuss, R. Jaenicke, G. Kühner, H. Ringler, A. Weller, and F. Wagner, Phys. Fluids B **4**, 2081 (1992).
[14] P. Xanthopoulos and F. Jenko, Phys. Plasmas **14**, 042501 (2007).
[15] W. Guttenfelder, D. T. Anderson, F. S. B. Anderson, J. M. Canik, K. M. Likin, and J. N. Talmadge, Phys. Plasmas **16**, 082508 (2009).
[16] V. Kornilov, R. Kleiber, R. Hatzky, L. Villard, and G. Jost, Phys. Plasmas **11**, 3196 (2004).
[17] N. Mattor, Phys. Fluids B **3**, 1913 (1991).